Supplemental Data

Contrasting Effects of the Persistent Na^+ Current on Neuronal Excitability and Spike Timing

K. Vervaeke, H. Hu, L.J. Graham, and J.F. Storm

Supplemental Figures

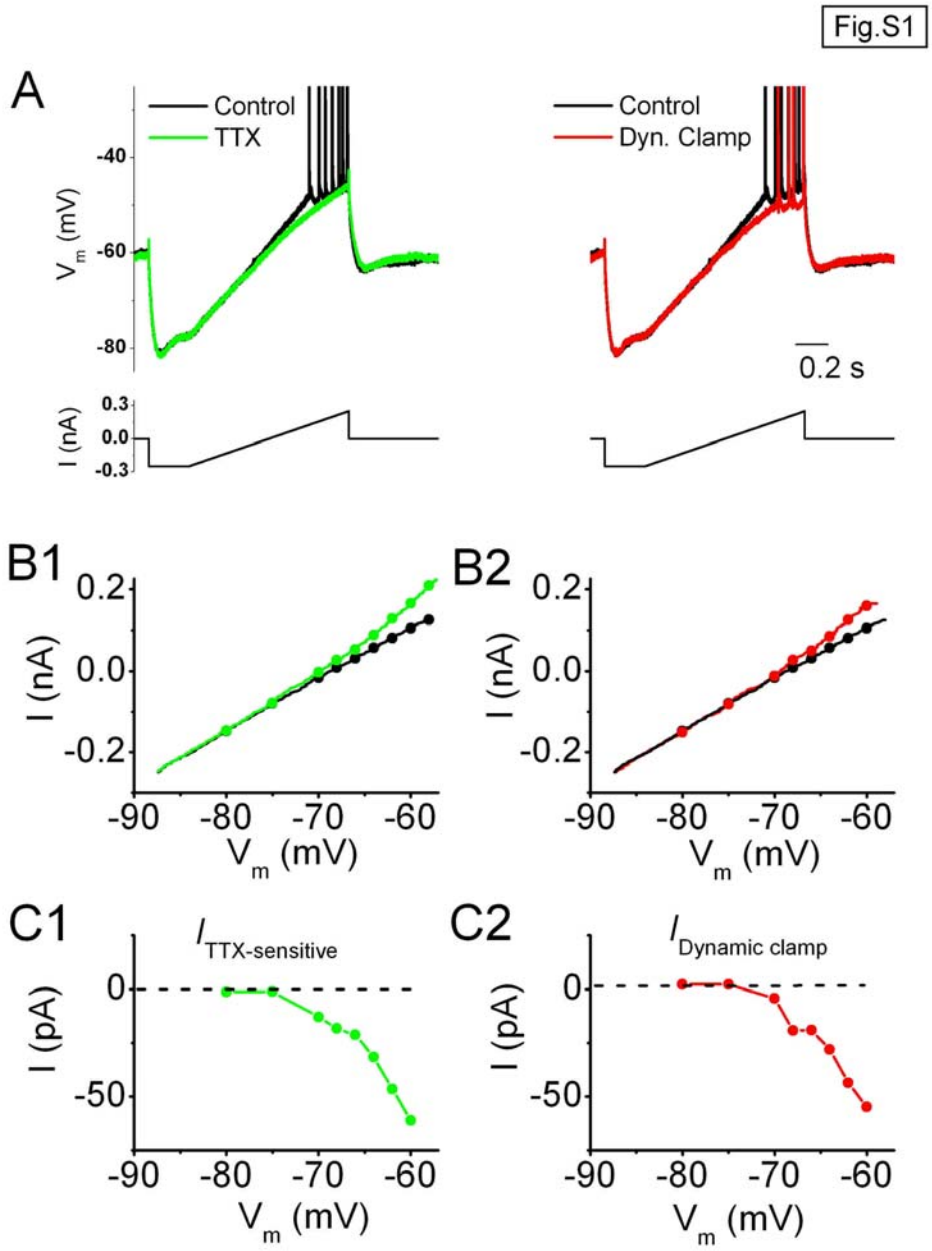

Fig.S1. Method for determining the voltage-dependence of I_{NaP} from current clamp data. (A) A current ramp (bottom traces) was injected into the cell and the voltage response recorded before and after application of TTX (left) or before and

after applying dynamic clamp (right) (i.e. same procedure as in Fig.2B). During the subthreshold parts of the responses, every value of injected current (*I*) corresponds to a certain value of the membrane potential (V_m). **(B1, B2)** The values of injected current (*I*) and V_m, taken from (A) are re-plotted, by plotting *I* as a function of V_m. **(C1)** and **(C2)** show the differences of the plots within B1 and B2, respectively, thus revealing the voltage dependence of the TTX-sensitive subthreshold current (C1) and dynamic clamp current (C2).

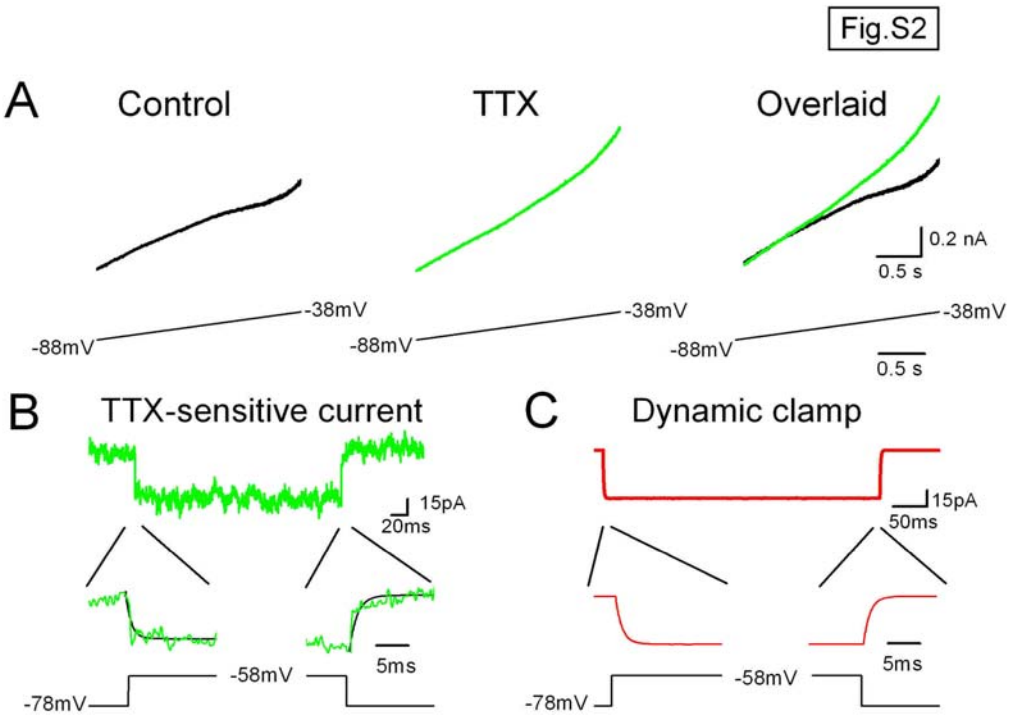

Fig.S2. Voltage clamp measurements of I_{NaP}. (**A)** During whole-cell voltage-clamp recording from a cell, a voltage ramp command (lower panels) was applied and the clamp current recorded before (black traces) and after adding TTX (green) (n=8, a summary of this type of data is plotted in Fig.2D). **(B)** A subthreshold voltage step was applied and the clamp current before and after TTX subtracted to obtain I_{NaP}. The activation and deactivation time courses of I_{NaP} were each fitted with a single exponential function. The time constants were 0.93 ± 0.14 ms and 0.99 ± 0.15 ms, respectively (n=4). **(C)** A similar voltage step protocol as in (B) was used to assess the speed of the artificial I_{NaP} generated by the dynamic clamp system in the open loop configuration. Here also, activation and deactivation were fitted with single exponential functions (time constants: 1.01 and 1.00 ms, respectively).

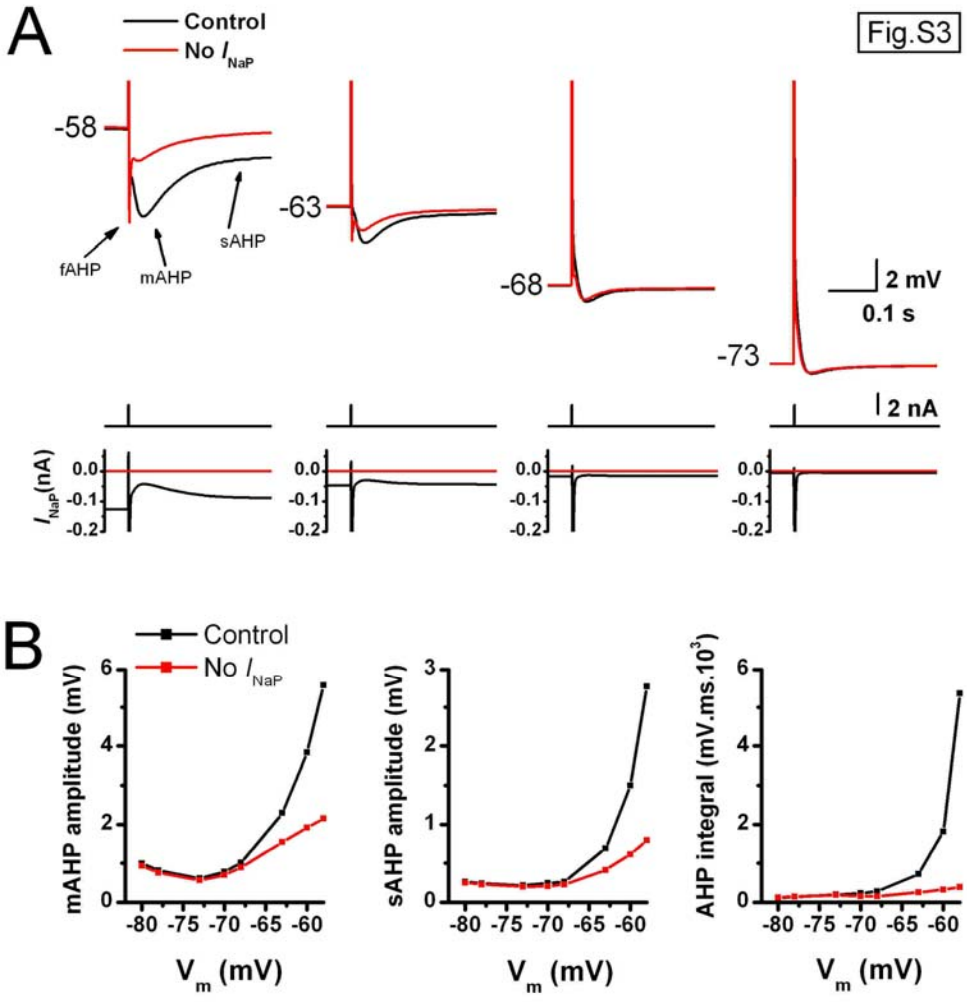

Fig.S3. Model simulations demonstrating voltage dependent amplification of AHPs by I_{NaP}. (A) Upper traces show single action potentials evoked with a short current pulse (middle panels, 2 nA, 1 ms duration) at different holding potentials, giving rise to a sequence of three types of AHPs; the fAHP, mAHP and sAHP, as indicated (action potentials are truncated). A constant current was injected in order to hold the membrane potential at indicated levels. Control voltage response (black) and the response when I_{NaP} was removed (red) were superimposed at each holding potential. The I_{NaP} response is shown in the lower panels for each case. **(B)** Summary data shows the voltage dependence of the mAHP amplitude (left panel), sAHP amplitude (middle panel) and total AHP integral (right panel) in control case (black) and when I_{NaP} is removed (red).

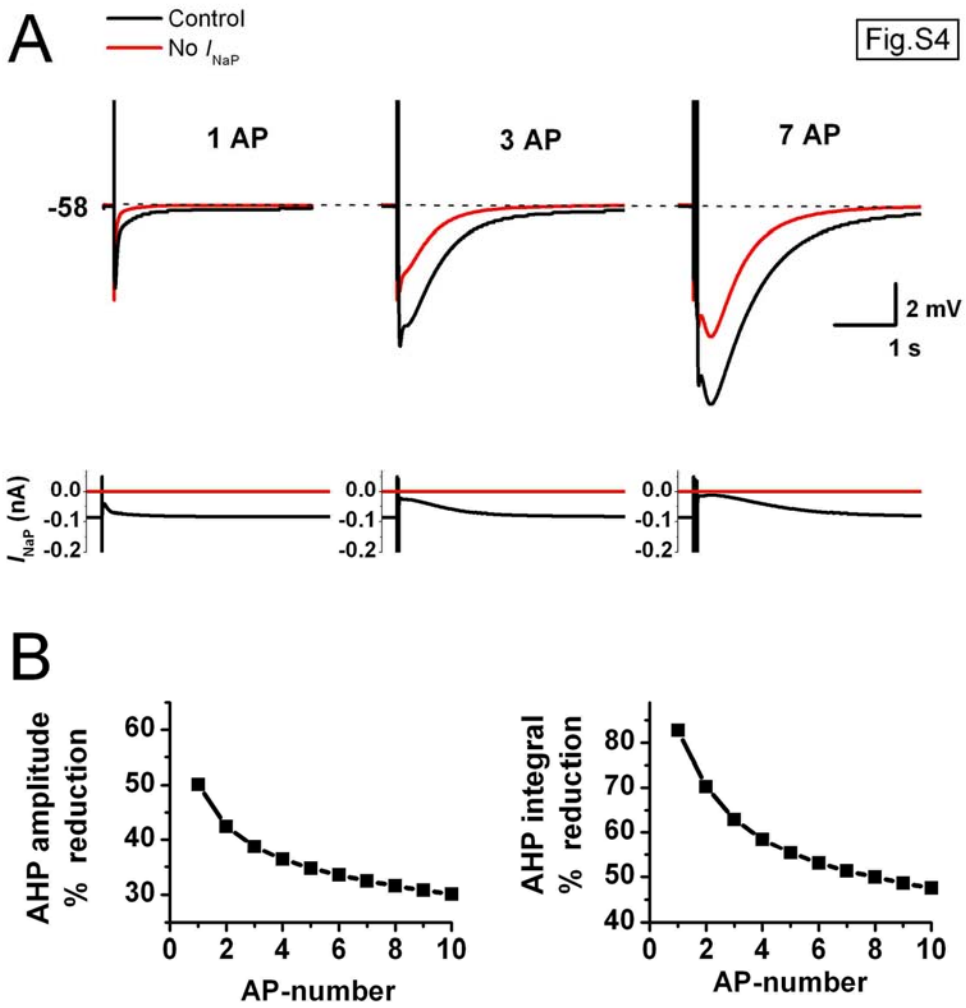

Fig.S4. Model simulations demonstrating the dependence of AHP amplification on AHP amplitude. (A) Increasing the number of action potentials gives rise to increasing AHPs (upper traces, action potentials are truncated). In all cases the membrane potential was held at –58 mV close to firing threshold with a constant current. Action potentials were elicited with short current pulses (100 Hz, 1 nA, 1 ms duration). The number of action potentials used for eliciting the AHPs is indicated. For each case the control voltage response (black) and the response when I_{NaP} is blocked (red) are superimposed. The I_{NaP} response is indicated in the lower panels. **(B)** Summary diagrams show how blocking I_{NaP} reduces the AHP amplitude (left panel) and AHP integral (right panel) as a function of the number of action potentials.

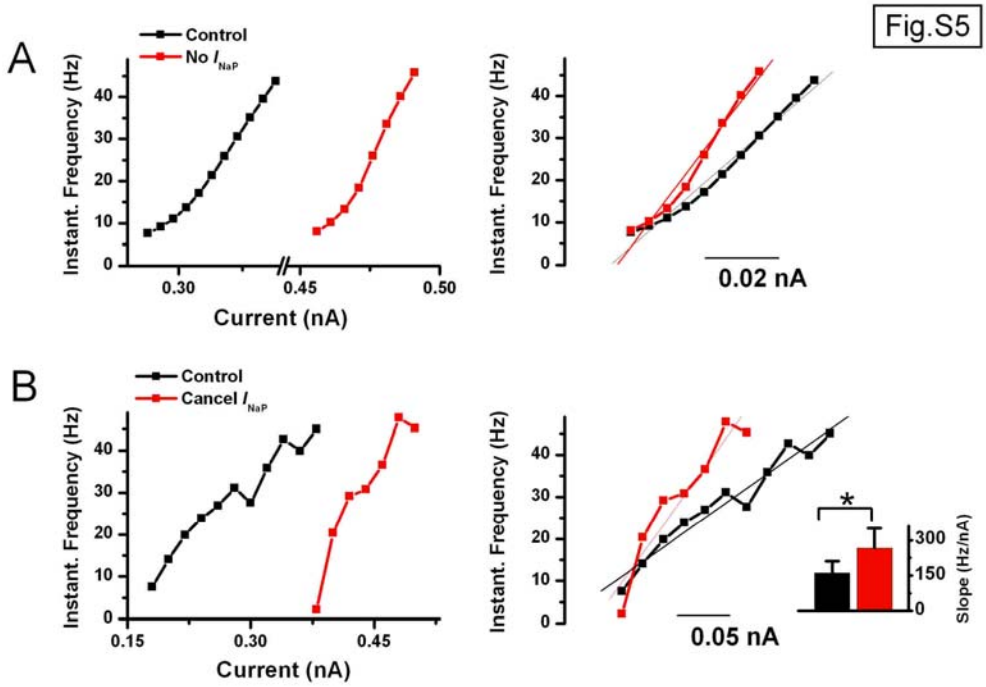

Fig.S5. **Model simulations and experimental results showing the effect of I_{NaP} on current-to-spike frequency transduction for the first ISI. (A)** Frequency-current (*f/I*) plots with I_{NaP} (black; Control) and without I_{NaP} (red) in the model. The instantaneous frequency is plotted for the first inter-spike interval in the spike train (1/first ISI) in response to injection of rectangular current pulses (1s duration, 5pA increments). The *f/I* slope increased by 44 % when I_{NaP} was blocked, as shown by the superimposed *f/I* plots fitted with a linear function (upper right panel). **(B)** Electrophysiological *f/I* plots (1/first ISI) recorded from a CA1 pyramidal cell according to the protocol described in (A), before (black) and after (red) canceling I_{NaP} by dynamic clamp. Linear fits of the *f/I* curves (right panels) showed that canceling I_{NaP} caused a clear increase in the *f/I* slope. On average the *f/I* slope increased by 65 % for all cells tested (n=7, $*$ p=0.03).

Supplemental Tables

Supplemental Table 1: Holding current at different membrane potentials with and without I_{NaP}

	Computer Modelling		Experiments	
	With I_{NaP} (nA)	Without I_{NaP} (nA)	Control (nA)	Cancel I_{NaP} (nA)
at -58mV	0.26	0.39	0.16±0.04	0.21±0.04
at -60mV	0.25	0.34	NA	NA
at -63mV	0.23	0.28	0.08±0.05	0.10±0.04
at -68mV	0.16	0.18	0.00±0.06	0.01±0.05
at -70mV	0.13	0.14	NA	NA
at -73mV	0.07	0.07	-0.08±0.06	-0.08±0.06
at -78mV	-0.03	-0.03	NA	NA
at -80mV	-0.08	-0.08	NA	NA

NA: not applicable

Supplemental Table 2: Number of action potentials to evoke an AHP at different membrane potentials

	Computer Modelling	Experiments
at -58mV	4	5.8±1.35
at -60mV	5	NA
at -63mV	7	7.0±0.81
at -68mV	9	7.6±1.12
at -70mV	12	NA
at -73mV	14	8.0±0.94
at -78mV	18	NA
at -80mV	23	NA

NA: not applicable

Supplemental Experimental Procedures

Slice preparation and whole cell recording

Male, 4-10 weeks old Wistar rats were anesthetized with an intra-peritoneal injection of Equithesin (3 ml/kg body weight), before being perfused transcardially with ice-cold modified cutting solution (in mM): 230 sucrose, 25 $NaHCO_3$, 1.25 KCl, 1.25 KH_2PO_4, 7 $MgCl_2$, 1 $CaCl_2$, 25 glucose, and saturated with 95 % O_2 – 5 % CO_2. After decapitation, transverse hippocampal slices (300-400 μm) were prepared with a HR2 vibratome (Sigmann Elektronik, Germany) and stored submerged, at room temperature, in a solution (aCSF) containing in (mM): 125 NaCl, 25 $NaHCO_3$, 1.25 KCl, 1.25 KH_2PO_4, 1 $MgCl_2$, 1 $CaCl_2$, 25 glucose, and saturated with 95 % O_2 – 5 % CO_2. During recording, slices were submerged in aCSF with 2 mM $CaCl_2$ at 30-35 °C (<0.5 °C variation within each recording).

Dagan BVC 700A amplifiers (Minneapolis, USA) were used for current-clamp and Axonpatch 1D (Molecular Devices Corporation) for voltage-clamp recording. Whole-cell recordings were obtained from CA1 pyramidal neurons visualized by an upright microscope (Olympus, BX50 with IR-DIC). The patch pipettes were filled with solution containing (in mM): 140 K-gluconate or $KMeSO_4$, 10 HEPES, 2 ATP, 0.4 GTP, 2 $MgCl_2$, 10 phosphocreatine, giving a pipette resistance of 2-5 MΩ for somatic recording and 8-12 MΩ for dendritic recording. The series resistance was 15-60 MΩ, and all potentials were corrected for the junction potential (-8 to -10 mV).

In Fig.7, to evoke EPSPs, a glass pipette filled with extracellular solution was placed in the middle of *stratum radiatum* of the CA1 area, ~200 μm from the site of recording (stimulation intensity: 100 μs, 10-200 μA). Bicuculline free base (10 μM) was routinely added to the extracellular medium to block inhibitory synaptic responses.

In Fig.4A, AHPs were simulated by injecting an AHP current waveform of the following format: $I_{AHP} = A\ [-0.09\ t\ \exp(-t / 19.20) + -0.01\ t\ \exp(-t / 250.54) + -0.0025\ t\ \exp(-t / 752.24) + 783\ 10^{-6}\ t\ \exp(-t / 943.18)]$, with t (ms), and "A" is an amplitude scaling factor. In Fig.7E,F somatic EPSPs were simulated by injecting an EPSC waveform into the apical dendrite (20-80% rise-time = 158 μs, τ_{decay1} = 2.55 ms, τ_{decay2} = 0.61 ms (Forti et al., 1997).

The experimental procedures are in accordance with the statute regulating animal experimentation, given by the Norwegian ministry of agriculture.

Dynamic Clamp

The steady state activation curve of I_{NaP} was based on our previous voltage clamp measurements in CA1 pyramidal neurons (Hu et al., 2002) and agrees well with other experimental reports (French et al., 1990;Crill, 1996). Initially, a G_{max} for I_{NaP} was determined from previous voltage clamp data (Hu et al., 2002) and the determination of this value was further refined by I_{NaP} subtraction and rescue experiments as shown in Fig.2. In pilot experiments, G_{max} was increased from 4-6 nS in steps of 0.4 nS and the G_{max} value (4.8 nS) that could most reliably cancel and restore the intrinsic I_{NaP} was used for further analysis (see Fig.2D). Somatic whole-cell voltage clamp measurements were used to assess the time-constants of I_{NaP} activation and

deactivation in the subthreshold range (Fig.S2B). A 250 ms long voltage step from -78 to -58 mV was applied and the clamp current before and after TTX application subtracted to obtain I_{NaP}. (n=4, Fig.S2B). Using pCLAMP 9 (Molecular Devices Corporation) the activation and deactivation time courses of I_{NaP} were each fitted with a single exponential function. The best fits had time constants of ~1 ms (0.93±0.14 ms and 0.99±0.15 ms, respectively; n=4). Therefore, voltage-independent activation- and deactivation time-constants of 1 ms were used for further analysis. To test the response speed of the dynamic clamp system we applied a voltage step from -78 to -58 mV in the open loop configuration and fitted the response with single exponential functions (Fig.S2C) giving activation and deactivation time constants of 1.01 and 1.00 ms respectively. To test whether I_{NaP} is localized peri-somatically, we repetitively applied a voltage step from -78 to -58 mV through a somatic recording electrode and monitored the steady state inward current. After a stable baseline, extra-cellular medium with 1 μM TTX and 0.2 V% fast green (Sigma) was locally pressure ejected to the soma with a micro-pipette (n=4) (the dye spread ~100 μm perpendicular to the somatic layer). The amplitude of the steady-state TTX-sensitive current, which was obtained by either local puffing or bath application of 1 μM TTX (n=4 in each case) showed no significant difference. Furthermore, local puffing occluded the effect of subsequent bath application of TTX (n=2; data not shown). Recordings from nucleated patches were tried, but they did not show any I_{NaP}. Except for the recordings of Fig.5B,C and Fig.7 (throughout which the bridge balance was carefully adjusted), V_m measurement and current injection were always performed through two separate patch electrodes, both in whole-cell configuration at the soma. Two separate electrodes were used in order to avoid any errors in the bridge balance, and hence inaccurate voltage recording, caused by non-linear or variable electrode resistance during large current injections.

Supplemental Computational Methods

Computer simulations were performed using the Surf-hippo neuron simulator, version 3.5a (Graham LJ, 2004). Surf-Hippo is written in Lisp and was run on a Linux workstation. For integrating the circuit equations, Surf-Hippo uses a variant of the Crank Nicholson method as described by Hines (Hines, 1984). The variable time-step method was used to speed up the simulations (Borg-Graham, 2000), with a maximum voltage error criterion of 0.05 mV.

We used a computer model that is derived from the Borg-Graham CA1 pyramidal neuron model (Borg-Graham, 1999), which has been refined through collaborative studies by using our experimental data on discharge patterns, AHPs, sub-threshold resonance and oscillations (Shao et al., 1999;Hu et al., 2002;Gu et al., 2005). This model reproduces quite accurately the spiking behaviour of these neurons (cf. Shao et al. 1999) as well as the AHPs following single action potentials or spike trains (Gu et al., 2005). We refer basically to the full description of the model in (Borg-Graham, 1999), and below we report the updated parameters.

The cell was represented by 5 compartments, comprising an isopotential soma (diameter 20 μm) and a dendritic cable (total length 800 μm and diameter 5 μm) consisting of 4 segments of equal length. Dendritic spines were not explicitly modelled but their contribution to the linear dendritic load was modelled by raising the dendritic segment capacitance and reducing the dendritic membrane resistance (Rall et al., 1992). The soma and the dendritic segments had a membrane resistance of 20 and 6 $k\Omega.cm^2$, respectively, while the capacitance was 1.0 and 1.5 $\mu F/cm^2$. A uniform intracellular resistance of 100 Ω.cm was assumed (Stuart and Spruston, 1998). With these values the model was able to account for the input resistance and whole-cell capacitance measured in our experiments. The active conductances included persistent and transient Na^+ currents (I_{NaP}, I_{NaT}) (Borg-Graham, 1999), 4 voltage-gated potassium currents I_A, I_D, I_{DR}, I_M, a fast inactivating BK-type Ca^{2+}- and voltage-dependent K^+ current I_{BK} (Shao et al., 1999), two voltage gated calcium currents I_{CaN} and I_{CaL}, a hyperpolarization-activated non-specific cation current I_h and a Ca^{2+} activated sAHP current (I_{sAHP}) (Borg-Graham, 1999).

The soma is divided into 3 sub-cellular compartments to model the differential and localized intracellular Ca^{2+} dynamics. The outer membrane shell consists of two juxta-membrane shells to reproduce the Ca^{2+} channel dependence of the BK- and sAHP current, in particular a co-localization of the channels underlying I_{CaN} and I_{BK} (Borg-Graham, 1987). The rest of the somatic volume is occupied by a core compartment. As Ca^{2+} ions enter through the calcium channels they diffuse among the sub-cellular compartments and undergo instantaneous buffering while a Ca^{2+} pump causes efflux of Ca^{2+} ions into the extra-cellular space. $[Ca^{2+}]$ in all compartments was initially set to 50 nM.

Calculation of all currents was based on the extended Hodgkin-Huxley formalism (see below) with rate constants derived from a single-barrier thermodynamic gating particle model (Borg-Graham, 1987). Exceptions are I_{NaT} and I_{BK}, which were calculated according to a more generalized Markov scheme (Shao et al., 1999;Borg-Graham, 1999). In the I_{NaT} Markov model, during an action potential the inactivation

state *I* is reached primarily from the activation (open) state *O*. This activation-inactivation sequence, in contrast to the decoupled activation and inactivation in the classical Hodgkin-Huxley formulation, allows essentially independent adjustment of the steady-state or persistent component of the model. Successive closed states, *C1* and *C2*, respectively, are reached from the inactivation state with progressively larger membrane hyperpolarizations after the spike. The open state may be reached from either closed state, with a voltage dependence that parallels the path into the respective closed state. This gives a range of thresholds such that more hyperpolarized pre-potentials provide successively lower thresholds for subsequent spikes. Simulations were performed based on a temperature of 30 °C.

All currents except for I_h were confined to the soma. Although many studies have shown that the dendrites are endowed with a complex repertoire of ion channels several lines of experimental evidence support this choice of distribution as a good approximation for studying somatic discharge patterns and AHPs in response to somatic input.

In CA1 pyramidal neurons voltage recordings of more distal dendritic action potentials rarely show any substantial AHPs, even though a significant Ca^{2+} influx can be recorded (Spruston et al., 1995;Andreasen and Lambert, 1995a;Magee and Johnston, 1997;Tsubokawa and Ross, 1997;Poolos and Johnston, 1999), but see (Andreasen and Lambert, 1995b). Furthermore, any AHP that is present in the dendrites is usually sensitive to I_h blockers (Magee, 1998). Ca^{2+} dependent K^+ currents have not been directly recorded from CA1 pyramidal dendrites. However we can infer from more indirect data that the density of these channels is very low in the distal dendrites. Also, as predicted by modelling studies (Borg-Graham, 1987), BK channels have been reported to co-localize with N-type calcium channels (Marrion and Tavalin, 1998) and the I_{sAHP} is largely reduced by dihydropyridines that block L-type channels (Borde et al., 2000). The lower N- and L-type channel densities present in the distal dendrites (Magee and Johnston, 1995;Christie et al., 1995;Kavalali et al., 1997) may explain why BK and I_{sAHP} activity is scarce in these regions. The Ca^{2+} current of the more proximal regions of the cell appears to be carried predominantly by L-type and N-type channels while Ni^{2+} sensitive channels (T- and R- types) appear to play a more dominant role in the distal regions of the cell.

Recent evidence indicate that KCNQ2 subunits are concentrated at the initial segment and axon nodes of CA1 pyramidal cells (Devaux et al., 2004). Since KCNQ2/KCNQ3 heteromers probably underlie a major component of the M-current in CA1 pyramidal cells (Wang et al., 1998) it seems reasonable, as a first approximation, to confine I_M to the somatic compartment.

The A-current (I_A) density along the apical dendritic trunk has been shown to increase linearly with distance from the soma (Hoffman et al., 1997). However, simulations with different I_A distributions in our model indicated that this parameter was not critical to capture the firing behaviour known from experimental somatic recordings. We could reproduce the firing responses from these neurons quite accurately with an A-current restricted to the soma, see also (Shao et al., 1999;Borg-Graham, 1999;Gu et al., 2005).

Also I_h has been shown to increase linearly in the apical trunk away from the soma (Magee, 1998). Due to a higher leak conductance in the dendrites compared to the soma (Stuart et al., 1999) and the observation that the membrane potential does not differ significantly throughout the sub-cellular compartments of the cell (Magee, 1998;Pouille and Scanziani, 2004), made it necessary for us to distribute I_h also at a

higher density in the dendritic compartment of the model so all compartments of the model would be approximately equipotential.

The I_{NaP} current has been found both in the soma and dendrites, but most of it (> 50 % of the total current in voltage clamp, see French et al.) appears to be of perisomatic origin (French et al., 1990;Stuart and Sakmann, 1995), as has also been reported for neocortical (Stuart and Sakmann, 1995) and Purkinje neurons (Kay et al., 1998). Much of the Na^+ channels generating I_{NaP} might be targeted to the axon initial segment (Ruben PC et al., 2003). Furthermore, we tested the impact of the distribution of the I_{NaP} but found that different distribution profiles along the soma and dendrites did not produce any qualitative differences to our findings.

Finally, the D-current seems to be mainly in the soma or proximal dendrites (Golding et al., 1999;Bekkers and Delaney, 2001).

The extended Hodgkin Huxley Scheme:

A template for this scheme is now also provided in the NEURON simulator and is called, "Borg-Graham style".

$n_C \xleftarrow{\alpha(V),\beta(V)} n_o$ **(1)** , α(V) and β(V) being the forward and backward rate respectively

$$\frac{dn}{dt} = \frac{n - n_\infty(V)}{\tau_n(V)} \quad \textbf{(2)}$$

the EXT-H-H forward rate: $$\alpha_n'(V) = K \exp\left(\frac{z\ \gamma\left(V - V_{\frac{1}{2}}\right)F}{R\,T}\right) \quad \textbf{(3)}$$

the EXT-H-H backward rate: $$\beta_n'(V) = K \exp\left(\frac{-z\,(1-\gamma)\left(V - V_{\frac{1}{2}}\right)F}{R\,T}\right) \quad \textbf{(4)}$$

The time-constant and steady-state particle are then described by:

$$\tau_n(V) = \left(\frac{1}{\alpha_n'(V) + \beta_n'(V)}\right) + \tau_0 \quad \textbf{(5)} \qquad n_\infty(V) = \frac{\alpha_n'(V)}{\alpha_n'(V) + \beta_n'(V)} \quad \textbf{(6)}$$

Note: how to relate the EXT-H-H forward and backward rate-constants to the usual Hodgkin Huxley rate description :

$$\alpha_n(V) = \frac{\alpha_n'(V)}{\tau_0\left(\alpha_n'(V) + \beta_n'(V)\right) + 1} \quad \textbf{(7)} \qquad \beta_n(V) = \frac{\beta_n'(V)}{\tau_0\left(\alpha_n'(V) + \beta_n'(V)\right) + 1} \quad \textbf{(8)}$$

The persistent sodium current, I_{NaP}

(French et al., 1990;Stuart and Sakmann, 1995;Kay et al., 1998;Magistretti and Alonso, 1999;Taddese and Bean, 2002)

Model type: Extended Hodgkin Huxley

Channel density ($pS/\mu m^2$)	7	
E-rev (mV)	30	
Number of particles	1 activation particle	
	Activation particle	**Inactivation particle**
Valence, z	6	-
γ	0.5	-
V-half (mV)	-51	-
τ_0 (ms)	1	-
Base-rate, K (1/ms)	- (*)	-
Q10	2	-
Reference temperature (°C)	31	-

(*): If the entry for base-rate is missing, then $\tau_n(V)$ for the particle is determined by τ_0 and $n_\infty(V)$ is calculated with base-rate = 1.

The A-current, I_A

(Klee et al., 1995;Hoffman et al., 1997;Migliore et al., 1999;Pan and Colbert, 2001)

Model type: Extended Hodgkin Huxley

Channel density ($pS/\mu m^2$)	450	
E-rev (mV)	-70	
Number of particles	1 activation particle	3 inactivation particles
	Activation particle	**Inactivation particle**
Valence, z	5	-3
γ	0.85	1
V-half (mV)	9	-60
τ_0 (ms)	0.3	2
Base-rate, K (1/ms)	0.16	0.08
Q10	Not applicable	Not applicable
Reference temperature (°C)	Not applicable	Not applicable

The delayed rectifier current, I_{DR}

(Sah et al., 1988;Hoffman et al., 1997;Du et al., 2000)

Model type: Extended Hodgkin Huxley		
Channel density ($pS/\mu m^2$)	900	
E-rev (mV)	-90	
Number of particles	1 activation particle	1 inactivation particle
	Activation particle	**Inactivation particle**
Valence, z	5	-1
γ	0	0
V-half (mV)	-24	-68
τ_0 (ms)	3	300
Base-rate, K (1/ms)	0.06	-
Q10	3	3
Reference temperature (°C)	27	27

The D-current, I_D

(Storm, 1988;Golding et al., 1999;Wu and Barish, 1999;Mitterdorfer and Bean, 2002)

Model type: Extended Hodgkin Huxley		
Channel density ($pS/\mu m^2$)	10	
E-rev (mV)	-90	
Number of particles	1 activation particle	1 inactivation particle
	Activation particle	**Inactivation particle**
Valence, z	8	-5
γ	0	0
V-half (mV)	-53	-80
τ_0 (ms)	1	2
Base-rate, K (1/ms)	-	2e-4
Q10	Not applicable	Not applicable
Reference temperature (°C)	Not applicable	Not applicable

The M-current, I_M

(Halliwell and Adams, 1982;Cooper et al., 2001;Hu et al., 2002;Devaux et al., 2004)

Model type: Extended Hodgkin Huxley		
Channel density ($pS/\mu m^2$)	7	
E-rev (mV)	-80	
Number of particles	1 activation particle	
	Activation particle	**Inactivation particle**
Valence, z	6	
γ	0.4	
V-half (mV)	-50	
τ_0 *(ms)*	1	
Base-rate, K (1/ms)	0.007	
Q10	5	
Reference temperature (°C)	35	

The h-current, I_h

(Gasparini and DiFrancesco, 1997;Magee, 1998;Hu et al., 2002)

Model type: Extended Hodgkin Huxley		
Channel density ($pS/\mu m^2$)	0.1 at soma	1 at each segment
E-rev (mV)	-45	
Number of particles	1 activation particle	
	Activation particle	**Inactivation particle**
Valence, z	-6	
γ	0.5	
V-half (mV)	-83	
τ_0 *(ms)*	4	
Base-rate, K (1/ms)	0.007	
Q10	5	
Reference temperature (°C)	32	

The L-type calcium current, I_{CaL}

(Westenbroek et al., 1990;Magee and Johnston, 1995;Christie et al., 1995;Kavalali et al., 1997). Ca^{2+} currents were not described using an ohmic model but instead by the Goldman-Huxley-Katz current equation.

Model type: Extended Hodgkin Huxley

Permeability (cm^3/s)	5 e-10
$[Ca^{2+}]_{extra}$	1.8 mM
$[Ca^{2+}]_{intra}$	50 nM
Number of particles	2 activation particles

	Activation particle	Inactivation particle
Valence, z	4.6	
γ	0	
V-half (mV)	-1.2	
τ_0 (ms)	1.5	
Base-rate, K (1/ms)	-	
Q10	Not applicable	
Reference temperature (°C)	Not applicable	

The N-type calcium channel, I_{CaN}

(Fisher et al., 1990;Magee and Johnston, 1995;Christie et al., 1995;Kavalali et al., 1997;Stuart et al., 1999). Ca^{2+} currents were not described using an ohmic model but instead by the Goldman-Huxley-Katz current equation.

Model type: Extended Hodgkin Huxley

Permeability (cm^3/s)	1 e-9	
$[Ca^{2+}]_{extra}$	1.8 mM	
$[Ca^{2+}]_{intra}$	50 nM	
Number of particles	2 activation particles	1 inactivation particle

	Activation particle	Inactivation particle
Valence, z	3.4	-2
γ	0	0
V-half (mV)	-21	-40
τ_0 (ms)	1.5	75
Base-rate, K (1/ms)	-	-
Q10	Not applicable	Not applicable
Reference temperature (°C)	Not applicable	Not applicable

The transient sodium current, I_{NaT}

The kinetics are described and motivated in (Borg-Graham, 1999).

The transition rate α_{ij} from state i to j, is defined by a squashed exponential of the form: $\alpha_{ij}(V) = \left(\tau_0 + \left(\alpha_0 + \exp\left(\frac{(V - V_{1/2})}{k} \right) \right)^{-1} \right)^{-1}$

current density (pS/μm^2)	900
E-reversal (mV)	65
Q10	Not applicable
reference temperature (°C)	Not applicable

	$V_{1/2}$ (mV)	k (mV)	α_0 (1/ms)	τ_0 (1/ms)
C2 O	-49.0	1		1/3
O C2	-57.0	-2.0		1/3
O I				*
O C1	-51.0	-2.0		1/3
C1 O	-42.0	1.0		1/3
I C1	-53.0	-1.0	0	1.0
C1 C2	-60.0	-1.0	0	1.0

** this transition rate is a constant: 3*

The BK type potassium current, I_{CT}

The kinetics are as described and motivated in (Borg-Graham, 1999),with updated parameters taken from (Shao et al., 1999).

Current-density (pS/μm^2): 130
E-rev: -80 mV

The sAHP current, I_{sAHP}

(Sah and Bekkers, 1996;Buhl et al., 1998;Bekkers, 2000;Borde et al., 2000;Vogalis et al., 2003)

current density (pS/μm^2):	7
E-rev (mV):	-95
concentration particles:	1
Alpha (ms^{-1}. mM^{-n}):	5e12
Beta (ms^{-1}):	0.01
τ_0 *(ms)*	250
n:	4
Q10:	Not applicable
reference temp (°C)	Not applicable

The Michaelis Menten Calcium extrusion pump

(motivated and described in (Borg-Graham, 1999))

v-max ($mM.s^{-1}$):	1.20e-10
Kd (mM):	0.02
Q10	Not applicable
reference temp (°C)	Not applicable

Reference List

Andreasen,M., and Lambert,J.D. (1995a). Regenerative properties of pyramidal cell dendrites in area CA1 of the rat hippocampus. J. Physiol *483 (Pt 2)*, 421-441.

Andreasen,M., and Lambert,J.D. (1995b). The excitability of CA1 pyramidal cell dendrites is modulated by a local Ca(2+)-dependent K(+)-conductance. Brain Res. *698*, 193-203.

Bekkers,J.M. (2000). Distribution of slow AHP channels on hippocampal CA1 pyramidal neurons. J. Neurophysiol. *83*, 1756-1759.

Bekkers,J.M., and Delaney,A.J. (2001). Modulation of excitability by alpha-dendrotoxin-sensitive potassium channels in neocortical pyramidal neurons. J. Neurosci. *21*, 6553-6560.

Borde,M., Bonansco,C., de Sevilla,F., Le Ray,D., and Buno,W. (2000). Voltage-clamp analysis of the potentiation of the slow Ca2+-activated K+ current in hippocampal pyramidal neurons. Hippocampus *10*, 198-206.

Borg-Graham,L. Modelling the somatic electrical behaviour of hippocampal pyramidal neurons. Master's thesis, Massachusetts Institute of Technology, Cambridge, MA, USA (also appears at MIT AI laboratory Technical report 1161). 1987.
Ref Type: Thesis/Dissertation

Borg-Graham,L. (1999). Interpretations of data and mechanisms for hippocampal pyramidal cell models. In Cerebral Cortex, volume 12: *Cortical models*, E.G. Jones, P.S. Ulinski, and A. Peter, eds. NY Plenum Press).

Borg-Graham,L.J. (2000). Additional efficient computation of branched nerve equations: adaptive time step and ideal voltage clamp. J. Comput. Neurosci. *8*, 209-226.

Buhl,E.H., Tamas,G., and Fisahn,A. (1998). Cholinergic activation and tonic excitation induce persistent gamma oscillations in mouse somatosensory cortex in vitro. J. Physiol *513 (Pt 1)*, 117-126.

Christie,B.R., Eliot,L.S., Ito,K., Miyakawa,H., and Johnston,D. (1995). Different Ca2+ channels in soma and dendrites of hippocampal pyramidal neurons mediate spike-induced Ca2+ influx. J. Neurophysiol. *73*, 2553-2557.

Cooper,E.C., Harrington,E., Jan,Y.N., and Jan,L.Y. (2001). M channel KCNQ2 subunits are localized to key sites for control of neuronal network oscillations and synchronization in mouse brain. J. Neurosci. *21*, 9529-9540.

Crill,W.E. (1996). Persistent sodium current in mammalian central neurons. Annu. Rev. Physiol *58*, 349-362.

Devaux,J.J., Kleopa,K.A., Cooper,E.C., and Scherer,S.S. (2004). KCNQ2 is a nodal K+ channel. Journal of Neuroscience *24*, 1236-1244.

Du,J., Haak,L.L., Phillips-Tansey,E., Russell,J.T., and McBain,C.J. (2000). Frequency-dependent regulation of rat hippocampal somato-dendritic excitability by the K+ channel subunit Kv2.1. J. Physiol *522 Pt 1*, 19-31.

Fisher,R.E., Gray,R., and Johnston,D. (1990). Properties and distribution of single voltage-gated calcium channels in adult hippocampal neurons. J. Neurophysiol. *64*, 91-104.

Forti,L., Bossi,M., Bergamaschi,A., Villa,A., and Malgaroli,A. (1997). Loose-patch recordings of single quanta at individual hippocampal synapses. Nature *388*, 874-878.

French,C.R., Sah,P., Buckett,K.J., and Gage,P.W. (1990). A voltage-dependent persistent sodium current in mammalian hippocampal neurons. J. Gen. Physiol *95*, 1139-1157.

Gasparini,S., and DiFrancesco,D. (1997). Action of the hyperpolarization-activated current (Ih) blocker ZD 7288 in hippocampal CA1 neurons. Pflugers Arch. *435*, 99-106.

Golding,N.L., Jung,H.Y., Mickus,T., and Spruston,N. (1999). Dendritic calcium spike initiation and repolarization are controlled by distinct potassium channel subtypes in CA1 pyramidal neurons. J. Neurosci. *19*, 8789-8798.

Graham LJ. The Surf-Hippo Neuron Simulation System, v3.5a. 2004. Ref Type: Computer Program

Gu,N., Vervaeke,K., Hu,H., and Storm,J.F. (2005). Kv7/KCNQ/M and HCN/h, but not KCa2/SK channels, contribute to the somatic medium after-hyperpolarization and excitability control in CA1 hippocampal pyramidal cells. J. Physiol *566*, 689-715.

Halliwell,J.V., and Adams,P.R. (1982). Voltage-clamp analysis of muscarinic excitation in hippocampal neurons. Brain Res. *250*, 71-92.

Hines,M. (1984). Efficient Computation of Branched Nerve Equations. International Journal of Bio-Medical Computing *15*, 69-76.

Hoffman,D.A., Magee,J.C., Colbert,C.M., and Johnston,D. (1997). K+ channel regulation of signal propagation in dendrites of hippocampal pyramidal neurons. Nature *387*, 869-875.

Hu,H., Vervaeke,K., and Storm,J.F. (2002). Two forms of electrical resonance at theta frequencies, generated by M-current, h-current and persistent Na+ current in rat hippocampal pyramidal cells. J. Physiol *545*, 783-805.

Kavalali,E.T., Zhuo,M., Bito,H., and Tsien,R.W. (1997). Dendritic Ca2+ channels characterized by recordings from isolated hippocampal dendritic segments. Neuron *18*, 651-663.

Kay,A.R., Sugimori,M., and Llinas,R. (1998). Kinetic and stochastic properties of a persistent sodium current in mature guinea pig cerebellar Purkinje cells. Journal of Neurophysiology *80*, 1167-1179.

Klee,R., Ficker,E., and Heinemann,U. (1995). Comparison of voltage-dependent potassium currents in rat pyramidal neurons acutely isolated from hippocampal regions CA1 and CA3. J. Neurophysiol. *74*, 1982-1995.

Magee,J.C. (1998). Dendritic hyperpolarization-activated currents modify the integrative properties of hippocampal CA1 pyramidal neurons. J. Neurosci. *18*, 7613-7624.

Magee,J.C., and Johnston,D. (1995). Characterization of single voltage-gated Na+ and Ca2+ channels in apical dendrites of rat CA1 pyramidal neurons. J. Physiol *487 (Pt 1)*, 67-90.

Magee,J.C., and Johnston,D. (1997). A synaptically controlled, associative signal for Hebbian plasticity in hippocampal neurons. Science *275*, 209-213.

Magistretti,J., and Alonso,A. (1999). Biophysical properties and slow voltage-dependent inactivation of a sustained sodium current in entorhinal cortex layer-II principal neurons - A whole-cell and single-channel study. Journal of General Physiology *114*, 491-509.

Marrion,N.V., and Tavalin,S.J. (1998). Selective activation of Ca2+-activated K+ channels by co-localized Ca2+ channels in hippocampal neurons. Nature *395*, 900-905.

Migliore,M., Hoffman,D.A., Magee,J.C., and Johnston,D. (1999). Role of an A-type K+ conductance in the back-propagation of action potentials in the dendrites of hippocampal pyramidal neurons. J. Comput. Neurosci. *7*, 5-15.

Mitterdorfer,J., and Bean,B.P. (2002). Potassium currents during the action potential of hippocampal CA3 neurons. J. Neurosci. *22*, 10106-10115.

Pan,E., and Colbert,C.M. (2001). Subthreshold inactivation of Na+ and K+ channels supports activity-dependent enhancement of back-propagating action potentials in hippocampal CA1. J. Neurophysiol. *85*, 1013-1016.

Poolos,N.P., and Johnston,D. (1999). Calcium-activated potassium conductances contribute to action potential repolarization at the soma but not the dendrites of hippocampal CA1 pyramidal neurons. J. Neurosci. *19*, 5205-5212.

Pouille,F., and Scanziani,M. (2004). Routing of spike series by dynamic circuits in the hippocampus. Nature *429*, 717-723.

Rall,W., Burke,R.E., Holmes,W.R., Jack,J.J., Redman,S.J., and Segev,I. (1992). Matching dendritic neuron models to experimental data. Physiol Rev. *72*, S159-S186.

Ruben PC, Ilschner SU, Williams SR, and Stuart GJ. Distribution and properties of sodium channels in the axon initial segment of layer 5 cortical pyramidal neurons. Society for Neuroscience . 2003.
Ref Type: Abstract

Sah,P., and Bekkers,J.M. (1996). Apical dendritic location of slow afterhyperpolarization current in hippocampal pyramidal neurons: implications for the integration of long-term potentiation. J. Neurosci. *16*, 4537-4542.

Sah,P., Gibb,A.J., and Gage,P.W. (1988). Potassium current activated by depolarization of dissociated neurons from adult guinea pig hippocampus. J. Gen. Physiol *92*, 263-278.

Shao,L.R., Halvorsrud,R., Borg-Graham,L., and Storm,J.F. (1999). The role of BK-type Ca2+-dependent K+ channels in spike broadening during repetitive firing in rat hippocampal pyramidal cells. J. Physiol *521 Pt 1*, 135-146.

Spruston,N., Schiller,Y., Stuart,G., and Sakmann,B. (1995). Activity-dependent action potential invasion and calcium influx into hippocampal CA1 dendrites. Science *268*, 297-300.

Storm,J.F. (1988). Temporal integration by a slowly inactivating K+ current in hippocampal neurons. Nature *336*, 379-381.

Stuart,G., and Sakmann,B. (1995). Amplification of EPSPs by axosomatic sodium channels in neocortical pyramidal neurons. Neuron *15*, 1065-1076.

Stuart,G., and Spruston,N. (1998). Determinants of voltage attenuation in neocortical pyramidal neuron dendrites. J. Neurosci. *18*, 3501-3510.

Stuart,G., Spruston,N., and Hausser,M. (1999). Dendrites.

Taddese,A., and Bean,B.P. (2002). Subthreshold sodium current from rapidly inactivating sodium channels drives spontaneous firing of tuberomammillary neurons. Neuron *33*, 587-600.

Tsubokawa,H., and Ross,W.N. (1997). Muscarinic modulation of spike backpropagation in the apical dendrites of hippocampal CA1 pyramidal neurons. Journal of Neuroscience *17*, 5782-5791.

Vogalis,F., Storm,J.F., and Lancaster,B. (2003). SK channels and the varieties of slow after-hyperpolarizations in neurons. European Journal of Neuroscience *18*, 3155-3166.

Wang,H.S., Pan,Z., Shi,W., Brown,B.S., Wymore,R.S., Cohen,I.S., Dixon,J.E., and McKinnon,D. (1998). KCNQ2 and KCNQ3 potassium channel subunits: molecular correlates of the M-channel. Science *282*, 1890-1893.

Westenbroek,R.E., Ahlijanian,M.K., and Catterall,W.A. (1990). Clustering of L-type Ca2+ channels at the base of major dendrites in hippocampal pyramidal neurons. Nature *347*, 281-284.

Wu,R.L., and Barish,M.E. (1999). Modulation of a slowly inactivating potassium current, I(D), by metabotropic glutamate receptor activation in cultured hippocampal pyramidal neurons. J. Neurosci. *19*, 6825-6837.